Precast TRC sandwich panels for energy retrofitting of existing residential buildings: full-scale testing and modelling

Isabella G. Colombo · Matteo Colombo · Marco di Prisco

Abstract In the 7th Framework Programme for Research and Technological Development, the European Commission financed the project EASEE (2012–2016), which was aimed at developing façade solutions for the energy retrofitting of multi-storey multi-owners existing residential buildings, built in an historical period in which no specific attention was paid to the energy issue. For the outer envelope, the consortium proposed textile reinforced concrete precast sandwich panels. The high durability, high aesthetic potential, low impact on occupant life during installation, and increase in impact resistance make this solution competitive with the exterior insulation and finishing system, now the most widespread energy retrofitting method adopted on existing buildings. Within the project, the panel has been mechanically investigated at multiple scales, and finally applied on some demo-buildings. This paper presents the investigation of the bending behavior of full-size panels up to failure when tested according to four-point bending scheme, focusing the attention on the effects of the production procedure and panel details on the structural behavior. The capability of expanded polystyrene in transferring shear stresses to the external TRC layers—already exhibited by specimens at lab-scale—is here verified on full-size elements. In addition, a numerical model—already validated for lab-scale sandwich beams—is here applied in order to check its reliability for the design of full-scale panel.

Keywords Textile reinforced concrete · Sandwich panel · Mechanical characterization · Four point bending test · Finite element model

I. G. Colombo (✉) · M. Colombo · M. di Prisco
Department of Civil and Environmental Engineering, Politecnico di Milano, Milan, Italy
e-mail: isabellagiorgia.colombo@polimi.it

M. Colombo
e-mail: matteo.colombo@polimi.it

M. di Prisco
e-mail: marco.diprisco@polimi.it

1 Introduction

In 2010, the European institutions took note that buildings are responsible for the 40% of total energy consumption in the Union. Hence, the Directive on the energy performance of buildings [1] promotes the improvement of the energy performance of new and existing buildings.

In the 7th Framework Programme for Research and Technological Development, the European Commission financed the project EASEE—Envelope Approach to improve Sustainability and Energy Efficiency in existing multi-storey multi-owner residential buildings. The project (2012–2016) concerned the retrofitting of multi-storey multi-owners existing residential buildings built between 1925 and 1975; those buildings were built in an historical period in

This is a post-peer-review, pre-copyedit version of an article published in Materials and Structures, 2019, 52:104. The final authenticated version is available online at: https://doi.org/10.1617/s11527-019-1406-1

which no specific attention was paid to the energy issue.

Within the project, three solutions were proposed: one for the inner envelope, one for the outer envelope and one for the wall cavity, when present.

Concerning the solution for the outer envelope, the consortium designed textile reinforced concrete (TRC) precast sandwich panels that could be a valid alternative to the exterior insulation and finishing system (EIFS), which is now the most widespread energy retrofitting method adopted on existing buildings.

The use of sandwich panels in buildings started in 1960s, when these products found large diffusion thanks to a worldwide growth in the prefabricated building element market [2]. One solution is constituted by R/C cladding sandwich panels, which are usually designed to act as partially or non-composite elements [3–5], in which concrete layers are connected through various type of shear connectors [6]. The thickness of the concrete layers, usually larger than 40 mm, entails a relevant weight of the precast elements.

About 10 years ago, German researchers [7] proposed lightweight TRC sandwich panels, which represent a new concept in the field of cement based sandwich elements. The use of TRC allows a significant reduction of the external layer thickness (15 mm) if compared to traditional panels, meaning a significant reduction in the weight of the structure. Additional advantages are the good durability and finishing, guaranteed by the use of fine-grained concrete. Even if connecting devices were introduced between the layers in order to guarantee a durable connection [8], adhesive bond between the insulation core and the TRC layers was exploited.

Further experiences on this kind of elements, characterized by external layers made of advances cementitious composite, have been performed in the last decade [9–16].

The prefabricated panel—designed within the EASEE project—is characterized by an inner insulation core, able to fit the energy requirement for the walls, and by external layers, obtained reinforcing a high strength mortar with an alkali-resistant glass fabric.

The main features of this panel are: its durability, the high aesthetic potential of the finishing, the low impact on occupant life during installation, and the increase in impact resistance.

In particular, a crane is used for the application on the existing façade, without the need of scaffolding; hence, the duration of the building site is limited, thus reducing the inconveniences for the inhabitants.

The high strength mortar is produced using thin aggregates (maximum aggregate size of 2 mm) and, eventually, color pigments; hence, a wide range of finishing can be obtained, guaranteeing, at the same time, a high durability thanks to the mortar performances and the core protected against atmospheric agents.

Large panels have been designed with the aim of minimizing the number, thus reducing the costs related to anchoring, and allowing the fixing to the R/C beams of the building.

In the framework of the project, the solution was applied on three demo buildings, including a three-story residential building in Cinisello Balsamo (Milano, Italy) [17], which was completely retrofitted with this solution.

A wide experimental campaign was performed in order to mechanically characterize the solution at different levels [18]: material [19], lab-scale [20] and real-scale (tests at SLS [21]). Then, analytical and numerical models were developed and validated at lab-scale in order to constitute a proper tool for the design of this kind of structure [22].

The durability of the solution has been also investigated. Concerning freezing and thawing, both TRC samples and sandwich beams were tested after the exposure to 500 cycles (− 18/+ 4 °C), considering both un-cracked and cracked condition [19, 23]; the effect on the real structure has been evaluated through the analytical model already validated, thus allowing the estimation of the reduction of the ultimate load. Concerning sun radiation, the effect of temperature variation on the mechanical behavior of the panel has been evaluated by means of the implemented numerical model [17]; the input temperatures come from a summer monitoring campaign performed on a west exposure test façade ($T_{max} = 40$ °C). It is worth noting that styrene-butadiene rubber (SBR) resin, which constitutes the coating of the fabric, maintains unchanged its mechanical properties up to 60 °C (data from the producer of the fabric).

In this paper, the experimental campaign on full-size elements is summarized. The investigation of the bending behavior of several panels up to failure when tested according to four-point bending scheme is discussed. The attention is focused on the effects of the production procedure and panel details on the structural behavior of the final element. The capability of expanded polystyrene in transferring shear stresses to the external TRC layers was already exhibited by specimens at lab-scale [20], and is here verified on full-size elements.

The numerical model—already validated for lab-scale sandwich beams [22]—is thus here applied in order to check its reliability for the design of full-scale panel.

2 Panel geometry, production and materials

The panel is characterized by a layered cross-section, with an internal expanded polystyrene (EPS) core and two external textile reinforced concrete (TRC) layers. The maximum size of the panel is equal to 1.5×3.3 m^2, which allows fixing it to the beams of the R/C frame of the building through four local connectors. These connectors are symmetrically placed in the panel (regions S1–S2–S3–S4; Fig. 1), by means of precast high-performance fiber reinforced concrete (HPFRC) boxes—$160 \times 120 \times 42$ mm—encapsulated into the insulation layer and embedded to the inner TRC layer.

To speed up the production of the panels for demo-buildings, two production technologies were used: a vertical casting procedure and a horizontal one.

The stratigraphy differs a little bit in the two cases due to technological issues (Fig. 1). The panels produced using a vertical formwork ("V") are characterized by textile reinforced concrete layers 12 mm thick and an expanded polystyrene core 100 mm thick, while panels produced through horizontal casting ("H") have external layers 14 mm thick and the core 96 mm thick. Also the edge detail is different, as shown in Fig. 1.

Expanded polystyrene is expected to transfer all the shear stresses to the TRC layers [20]. In any case, the panel is equipped by four stainless steel AISI 310S crimped bars ($\phi 5$) placed in the longitudinal panel edges at the upper and lower ends (Fig. 1) aimed at preventing the detachment of TRC layers in extreme conditions (e.g. fire). Each crimped bar was inserted in the EPS insulation panel before casting by imposing a manual pressure (Fig. 2); after casting, it remains embedded in both TRC layers.

EPS insulation panels were pre-cut in order to guest the HPFRC anchoring boxes (Fig. 2). After their placement, the AR-glass fabrics (one on each side) were fixed to the EPS mat by punctually gluing it on the EPS surface, thus resulting in contact with the insulation material (Fig. 2).

In case of vertical casting, the prepared EPS panel is introduced in the formwork and the mortar is cast from the top; spacers were fixed on the EPS surface in order to keep the insulation panel in the right position during casting (Fig. 2). In case of horizontal casting, the mortar of the outer TRC layer is cast on the bottom of the formwork; then, the prepared EPS panel is laid down on the mortar and finally the inner layer of mortar is cast.

In both cases, a high level of finishing is ensured thanks to the use a form liner placed on the formwork surface, reproducing the desired texture. The desired color could be obtained by adding pigments in the matrix mix.

The vertical casting was initially chosen in order to minimize voids and defects in the mortar and improve EPS/TRC and mortar/fabric bond. Previous experiences [20, 22] showed that this casting technique allows obtaining good bond between TRC and EPS in sandwich panels preventing any sliding, even when the behavior in bending becomes highly non-linear.

The matrix is characterized by fine aggregates (quartz sand with maximum particle size of 2 mm) and low water to binder ratio (0.19) [21]. It is self-compacting, with high flowability that guarantees good matrix-fabric and matrix-EPS bond. The average cubic compressive strength at 28 days is equal to 87.7 MPa (STD = 15.6% on 10 specimens) [24].

The leno-weave fabric used as reinforcement [21] is made of alkali-resistant glass coated with styrene-butadiene rubber (SBR). The spacing between yarns is equal to 10 mm and 14.3 mm respectively for warp and weft. Warp yarns run in the longitudinal direction of the panel. The nominal strength in the warp direction is equal to 680 MPa; it is computed as the ratio between the maximum average tensile load measured for 10 specimens 70 mm wide (9.15 kN on 7 yarns) and the equivalent cross-section area of glass (area of each yarn: 2×2400 Tex, corresponding to

Fig. 1 Test set-up with the instrumentation of the panel (measures in mm)

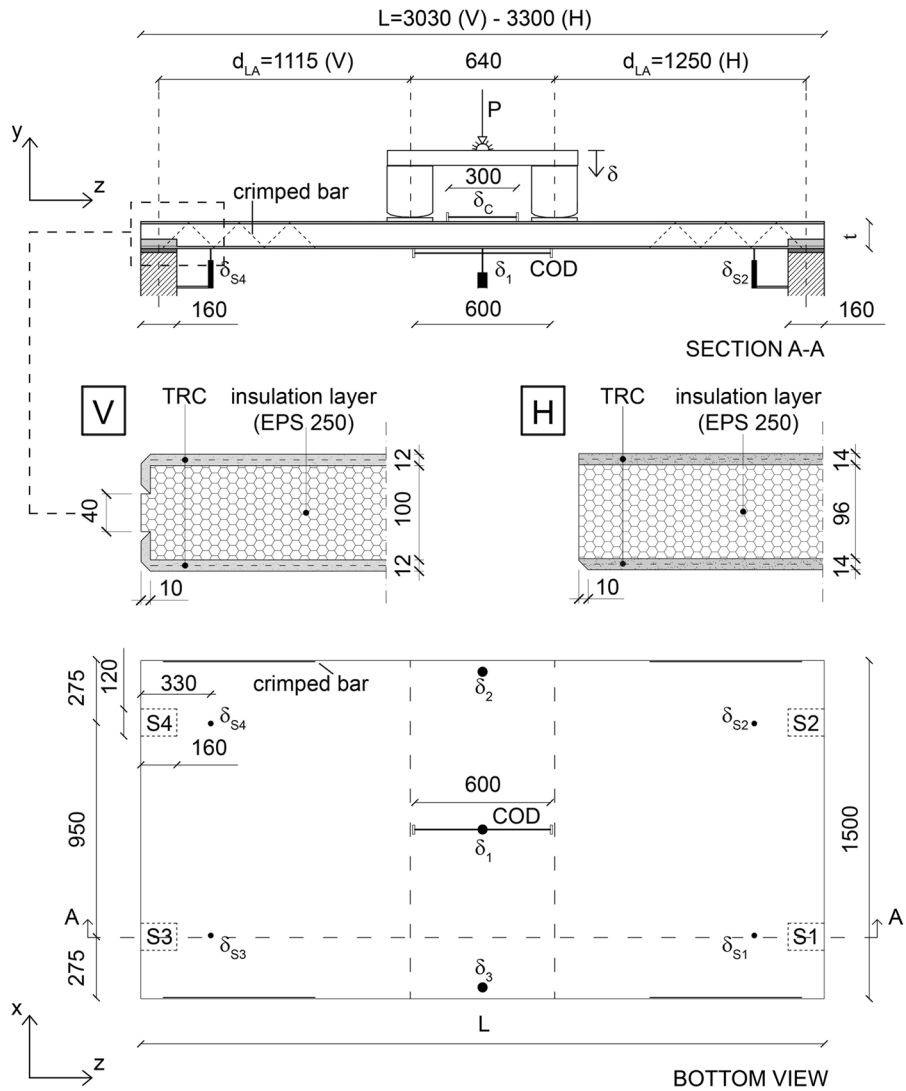

Fig. 2 Panel edge detail (V panel taken as reference)

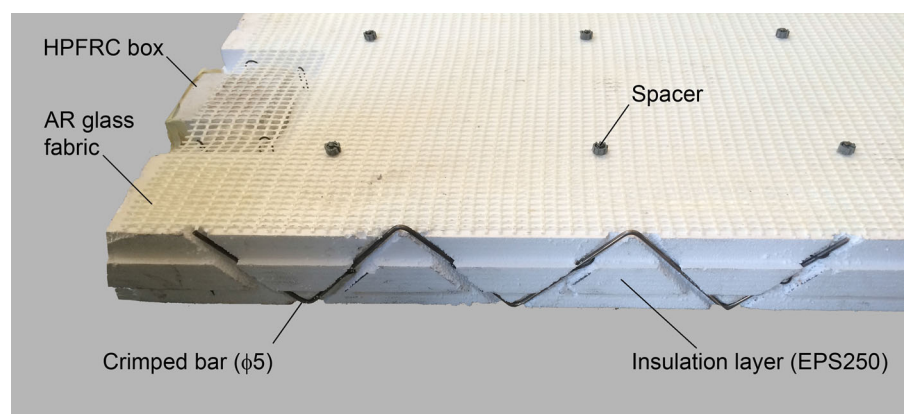

1.92 mm^2). Basing on previous experience [19, 25], this strength is expected to be constant in the operating environmental temperatures (− 18/+ 60 °C) as both the glass and the SBR coating keep their mechanical properties unvaried in this range.

The expanded polystyrene used is commercially known as "EPS250"; a nominal density of 35 kg/m^3 and a thermal conductivity of 0.034 W/mK [26] characterize it. According to the test results [22], the elastic modulus in compression is 13.7 MPa and the uniaxial compressive yield stress is 0.19 MPa, the uniaxial tensile yield stress (σ_{t_EPS}) is 0.39 MPa, the shear yield stress is 0.16 MPa and the shear modulus is 5.04 MPa.

3 Bending tests on full-scale panels

3.1 Experimental campaign

Four-point bending tests were performed on four full-scale panels, two produced using the vertical formwork ("V") and two cast horizontally ("H"). Repeatability equal to two was adopted. The specimen sizes are indicated in Fig. 1. It is worth noting that "H" panels are longer than "V" panels (3.30 m instead of 3.03 m) due to design aspects related to the application on the demo-building (beam distance in the concrete frame to which the panels are fixed). In addition, it has to be taken into account that "V" panels were previously tested at serviceability limit state (SLS) applying an increasing distributed load simulating the wind action.

These SLS tests [21] were performed placing the panels in horizontal position, fastening them on four points to two concrete supports by means of the real anchoring system designed for the panel, and loading them on the upper surface by filling a pool with water. The anchoring system consists of two main components: a body with a vertical slot, and a threaded spade bolt with a dowel pin, which is hosted in the HPFRC box that is precast and later embedded in the panel during the casting of TRC layers. Details of the anchoring system are shown in Colombo et al. [21] and not reported here for sake of brevity. The distributed load was applied on an area equal to 1.3 × 2.5 m^2. During these tests, a maximum bending moment of about 1.4 kNm was applied in the central cross-section of the panel. After the removal of the applied load, the global irreversible crack opening—measured astride the central cross-section of the panel in the gauge length of 450 mm—was equal to 0.8 mm and 0.6 mm respectively for the two specimens tested. In this region, multiple cracks arose, with a maximum residual crack width equal to 0.05 mm. It is worth noting that, at a level of pressure typical for SLS (1.50 kN/m^2), the global crack opening measured in the gauge length was equal to 135 μm and 34 μm respectively in the two cases: considering that multi-cracking occurred in this region, single crack width was smaller than 50 μm, meaning that cracks were not visible to the naked eye. [21]

Concerning four-point bending tests presented in this paper, the test set-up together with the instrumentation used for each panel is shown in Fig. 1. The panels were simply supported on four elastomeric bearing plates (160 × 120 × 10 mm) placed under the HPFRC boxes. Elastomeric plates made of neoprene were placed between the panel and the loading knives, in order to prevent load concentration.

The tests were displacement-controlled and carried out by using a contrast frame equipped with an electro-mechanical actuator (maximum capacity equal to 1000 kN), using the jack cross-head displacement (stroke) as feedback parameter and imposing a stroke rate equal to 15 μm/s.

The panel was instrumented as described in the following (Fig. 1, see both "section A–A" and "bottom view"):

- three potentiometric transducers were placed at mid-span, in vertical direction, in contact with the bottom surface of the panel, in order to measure the central deflections δ_1, δ_2 and δ_3;
- four inductive full-bridge linear variable differential transducers (LVDTs) were placed closed to support plates (S1, S2, S3, S4), in vertical direction, on the bottom surface of the panel, for measuring vertical displacements at supports δ_{S1}, δ_{S2}, δ_{S3} and δ_{S4};
- one inductive full-bridge LVDT was fixed on the bottom surface of the panel, astride the mid-span, with a nominal gauge length (L_{COD}) of 600 mm, to measure crack opening displacement (COD) in the mid-span region;
- another inductive full-bridge LVDT was placed on the upper surface of the panel, astride the mid-span, with a nominal gauge length (L_C) equal to

300 mm, aimed at measuring the displacement δ_C on the compressed side of the panel between the loading knives.

The measured gauge lengths ranged between 597 and 615 mm for L_{COD}, and between 293 and 305 mm for L_C.

The data acquisition is performed through an electronic measurement system with an acquisition rate of 1 Hz. The potentiometric transducers were characterized by a nominal displacement of 150 mm, and the inductive transducers were characterized by a nominal displacement of 10 mm. In order to prevent damages in the instrumentation equipment, the transducers were always removed before the specimen failure.

Due to an acquisition problem, the measurements of δ_1, δ_2 and δ_3 were not registered and are not available for "H" panels.

3.2 Experimental results

The load (P) versus stroke curves are shown for all the tested panels in Fig. 3: black dashed lines refer to V panels, and red continuous lines refer to H panels. The response of all the specimens showed a tri-linear behavior, which follows the tri-linear constitutive law of textile reinforced concrete in tension [27]. The initial slope of the first branch is related to the stiffness of the composite, which is strictly related to the stiffness of the cementitious mortar constituting the TRC layers. The second branch is characterized by the development of multiple cracks in the TRC layers, and, in the third branch, existing cracks widened up to the fabric failure in the lower TRC layer. In all the tests, the failure of the panel was driven by the failure of the bottom TRC layer. An acceptable repeatability is obtained for both types of panels.

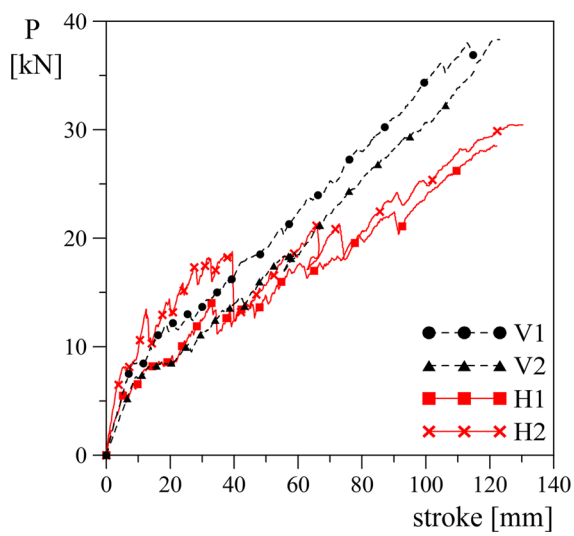

Fig. 3 Load versus stroke curves: experimental results

The ultimate load reached was equal to 39.0 kN and 35.9 kN respectively for panel V1 and V2, and to 28.7 kN and 30.7 kN respectively for panel H1 and H2. It is worth to note that it is not possible to directly compare the ultimate load of the two solutions, because the loading schemes differ of about 6% on the measured shear span.

The test results concerning V panels are plotted in Fig. 4 in terms of load (P) versus relative vertical displacement (δ^*) curves. The relative displacement is obtained subtracting the average vertical displacement at the supports (δ_S) from the value of the mid-point vertical displacement δ_1:

$$\delta_S = (\delta_{S1} + \delta_{S2} + \delta_{S3} + \delta_{S4})/4$$
$$\delta^* = \delta_1 - \delta_S$$

It is worth noting that the transducers were removed before the specimen failure to prevent any damage to the instrument equipment: hence, two horizontal dashed lines are plotted in the $P - \delta^*$ figure, thus indicating the level of the failure load.

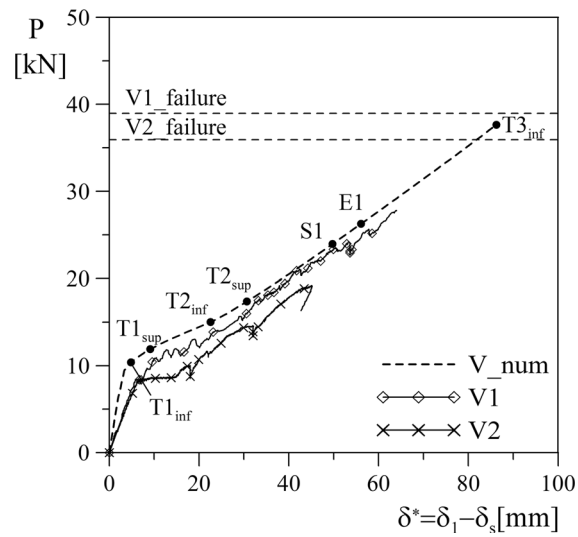

Fig. 4 Load versus vertical displacement curves: experimental and numerical results for V panels ("V_num" curve will be further explained in Sect. 4.3)

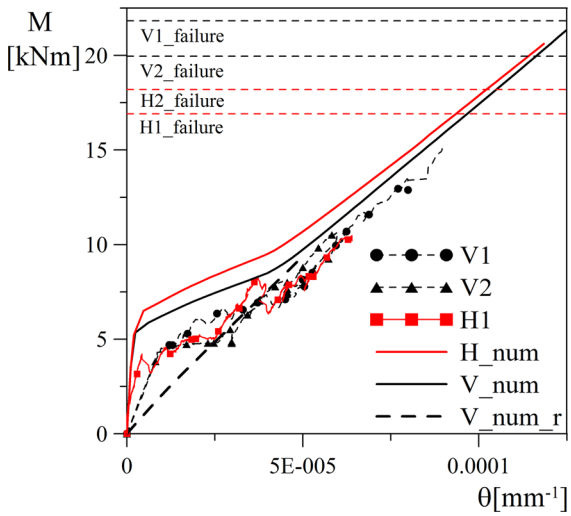

Fig. 5 Bending moment versus curvature curves: experimental and numerical results ("V_num", "V_num_r" and "H_num" will be further explained in Sect. 4.3)

The bending moment versus curvature curves are plotted in Fig. 5 for specimens V1, V2 and H1. The bending moment is computed multiplying $P/2$ by the effective shear span measured taking into account the support region middle axis, and the curvature, assuming plane sections, is defined as:

$$\vartheta = (\varepsilon_{COD} + \varepsilon_C)/t$$

with:

$$\varepsilon_{COD} = COD/L_{COD}$$
$$\varepsilon_C = \delta_C/L_C$$

L_{COD} and L_C represent the gauge lengths of the instruments devoted to measure respectively the crack opening displacement on the bottom surface of the panel and the longitudinal displacement of the compressed side; they are respectively nominally equal to 600 and 300 mm, but, in the computation of the curvature, the real values measured before each tests are used. When panel H2 was tested, crack-opening displacement was not correctly measured by the transducer; hence, the $M - \vartheta$ curve is not included in the figure.

Each curve was stopped when one of the displacement transducers reached its limit displacement or when the instrumentation was removed. Hence, in the figure, horizontal dashed lines are introduced in order to indicate the bending moment values corresponding to the failure load of the panels: these values are equal to 21.82 kNm, 19.96 kNm, 16.91 kNm and 18.20 kNm respectively for panel V1, V2, H1 and H2.

Comparing the bending moment-curvature curves for vertical and horizontal panels, it is possible to note that the initial slope of the H1 curve, which represent the bending stiffness of that panel, is considerably higher (8.5/10 times) than that of panels V1 and V2. This is in accordance with the expectation, as V panels have already been tested at serviceability limit state and, due to that, they were pre-cracked.

In the constant bending moment region (on which the crack opening displacement was measured) V and H panels are characterized by the same behavior (shown in Fig. 6a in terms of bending moment vs. crack opening displacement). In order to understand if a different sliding is occurring in the lateral regions (subjected to constant shear), the load versus average vertical displacement at supports is plotted in Fig. 6b. It is worth noting that, in these responses, the squeezing of neoprene at supports is included; however, this neoprene contribution just depends on the load level and is independent on the shear span. In the first and in the third branch of the curves, the panels present similar responses, also taking into account that the only small difference in the shear span should lead to a difference of about 5% on the displacement close to the supports. For this reason, it is possible to state that, in lateral regions, the behavior is not affected by the casting procedure neither by the edge detailing.

Concerning the second branch, it is possible to note that—as expected for H panels—the multi-cracking load level of specimen H2 is higher than that of V panels, due to the higher thickness of TRC layers. The same did not occur for panel H1, due to the early first-cracking possibly caused by the presence of defects.

In Fig. 6a, the un-loading and re-loading cycles performed on panel V1 in order to monitor permanent deformations are plotted (in the other graphs these cycles were not reported for a matter of clearness). During the measurement of COD, the specimen was un-loaded and re-loaded three times: the first one in the initial linear elastic branch, not leading to any residual crack opening, the second one at a bending moment level of 5.4 kNm and the third one at a value of 11.7 kNm. The irreversible COD measurement for the third cycle is equal to about 2 mm. Considering the large number of cracks (about 40) within the gauge length, this correspond to an average crack opening

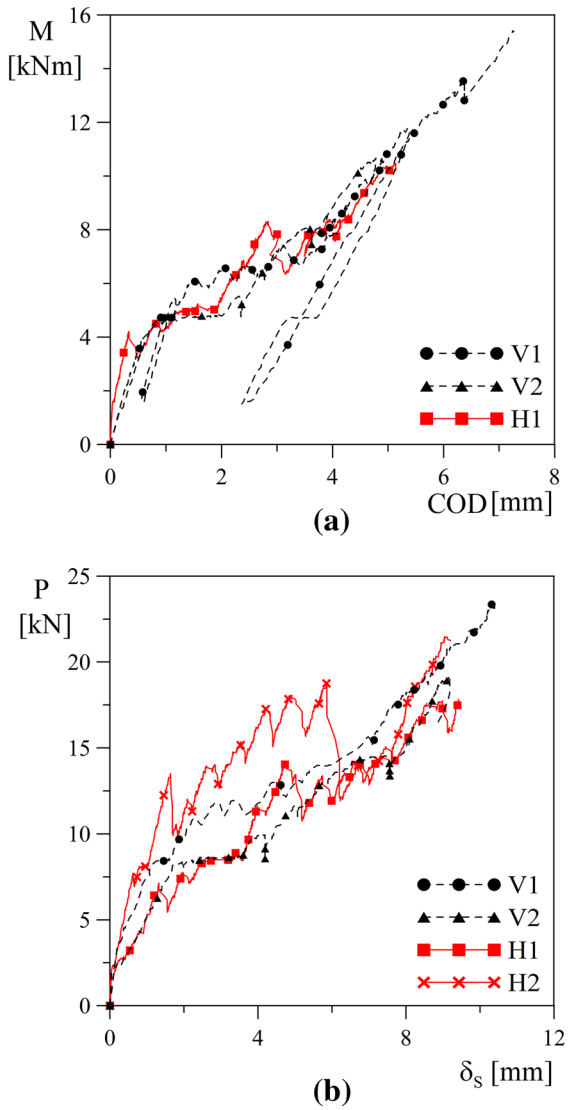

Fig. 6 Bending moment versus crack opening displacement curves (**a**) and load versus average vertical displacement at the supports (**b**)

close to 0.05 mm, that is significantly smaller than the usual limit adopted for crack control at SLS limit state. It is also important to point out that the bending moment at which this cycle is performed is significantly larger than the bending moment corresponding to wind action in SLS condition (e.g. $M_{SLS} \approx 2.6$ - kNm for a wind pressure of 1.5 kN/m^2).

In Fig. 7, two pictures of panel V2 are shown: subfigure (a) shows the panel during test, underlying the high deformability that characterizes this sandwich structure, and subfigure (b) is a zoom on the failure

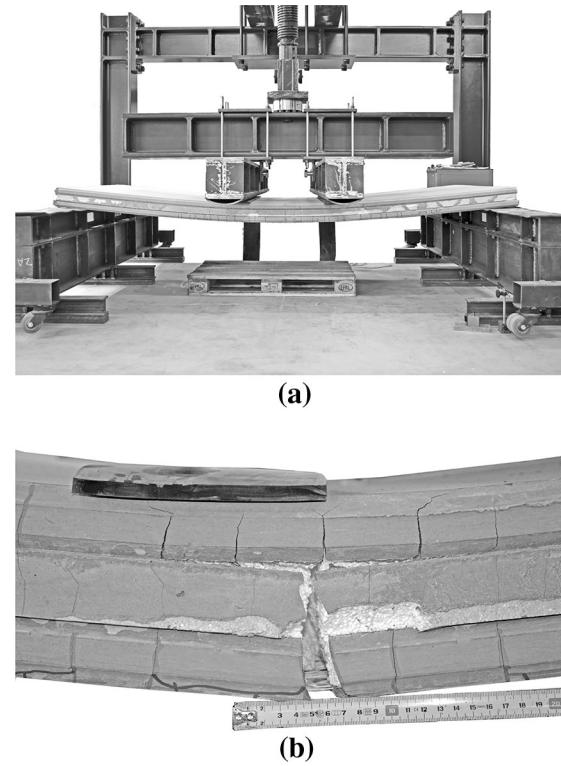

Fig. 7 Panel V2 during test (**a**) and after failure (**b**)

zone. In all the specimens, after a ductile behavior characterized by multi-cracking of both lower and upper TRC layers and, hence, a phase in which the multiple cracks widened, a sudden brittle failure occurred due to the reaching of the maximum tensile strength in the lower TRC layer. The failure of the bottom layer caused the propagation of the crack in the polystyrene layer and, then, the debonding between the EPS and the upper TRC layer.

The multi-cracking phenomenon mainly involves a large portion of the lower TRC layer (see Fig. 8), even if some cracks are also visible on the lateral side of the top TRC layer between the loading knives. This implies a behavior as partially composite sandwich, as already underlined for sandwich beams in Colombo et al. [22]. This means that the external layers are subjected not only to membrane action, but local bending moments are also available on the TRC layers.

Comparing the bottom crack patterns of V and H panels (Fig. 8), it is possible to note that much more cracks occurred in vertically cast panels. In particular, focusing on the constant bending moment region, in V

Fig. 8 Crack pattern on the intrados of each panel (blue dot-lines = pre-cracks due to SLS tests, with corresponding crack width values). (Color figure online)

panels a crack spacing corresponding to the weft distance can be observed (in both cases 41 cracks can be detected). Concerning H panels, in the same region, 10 and 14 cracks formed respectively in H1 and H2 panel, meaning that one crack every three or four weft yarns occurred. As the moment-COD response of the two solution is comparable (Fig. 6a), this means that, at the same load level, cracks in H panels should be wider than those in V panels.

In Colombo et al. [20] it was underlined that the crack spacing in sandwich beams was mainly related to the fabric position in the thickness of the TRC layer. In both V and H panels, the fabric in the TRC layers lays close to the EPS surface; taking into account that all the panels are characterized by the same global behavior (Fig. 6), the larger crack spacing measured in H panels could be correlated to the higher thickness of TRC layers, that reduces the geometrical reinforcement ratio of the layer of about 15%.

The different thickness implies a different energy release at crack formation. This may cause the different crack spacing in H and V panels and could be also related to the different ultimate bending moment at failure.

In the same Fig. 8, dot-lines highlight the cracks that could be detected in panels V1 and V2 before the tests, mainly due to SLS load-controlled bending tests.

4 Numerical modelling of the tests

Two numerical models have been built in Abaqus/CAE, one for the vertically cast and one for the horizontally cast panel. The aim is to predict the behavior of the sandwich panels and to clarify the mechanisms involved in their failure. The main features of the models are that material non-linear behavior is accounted, textile reinforced concrete is modeled as a homogeneous material [22] and perfect bond is assumed at TRC-EPS interfaces.

4.1 Description of the models

The two models have been built by exactly reproducing the stratigraphy and geometrical shape of each panel. Hence, they differ in terms of thickness of the layers and shape of the edges (see Fig. 1). With reference to the test set-up, the loading knives, the neoprene supporting plates and the neoprene pads laying in the loading region are included in the model. In order to limit the number of nodes and elements, and hence the numerical effort, each model reproduces just a quarter of the panel, taking advantage of *xy* and *yz* symmetries.

The geometry of the quarter of the panel (taking V as an example) is shown in Fig. 9a, in which also the constraints and the imposed displacement (δ) are indicated.

This vertical displacement δ is imposed overall the upper surface of the knife. In order to model the symmetries, the displacements orthogonal to the symmetry planes are prevented. The neoprene support is constrained in vertical direction on the bottom surface. In addition, some nodes of the knife (identified in Fig. 9a) are constrained in *z*-direction in order to prevent improper displacements of the loading device.

All the panel components (TRC layers, EPS layer and HPFRC boxes), the neoprene elements and the loading knife are modelled as solid and homogeneous elements, while the crimped bar is modelled as a truss. The crimped bar is fully constrained to the panel geometry by creating an embedded region that is hosted in both EPS and TRC layers. A node-to-node rigid kinematic link is provided between each bar node and the closest node in the hosting material. In the real panel, the crimped bars are embedded only in the concrete layers and not in the EPS layer; the assumption made in the numerical model could lead to a numerical response stiffer than the experimental one. However, a previous comparison of results on FE analysis with and without crimped bars showed that their influence on the panel global behavior results negligible, thus proving the reliability of such assumption.

Perfect bond is considered between TRC and EPS, between neoprene plates and TRC and between the HPFRC boxes and the mortar of the lower TRC layer. The knife, initially detached from the structure, is moved coming into contact with the upper neoprene plate, thus loading the panel.

Figure 9b shows the mesh: solid homogeneous sections are meshed through four-node linear tetrahedral elements (C3D4—Continuum, 3-D, 4-node), and truss representing the crimped bar is meshed through two-node linear truss elements (T3D2—Truss, 3-D, 2-node). All the mesh characteristics are collected in Table 1, including the number of nodes, number and

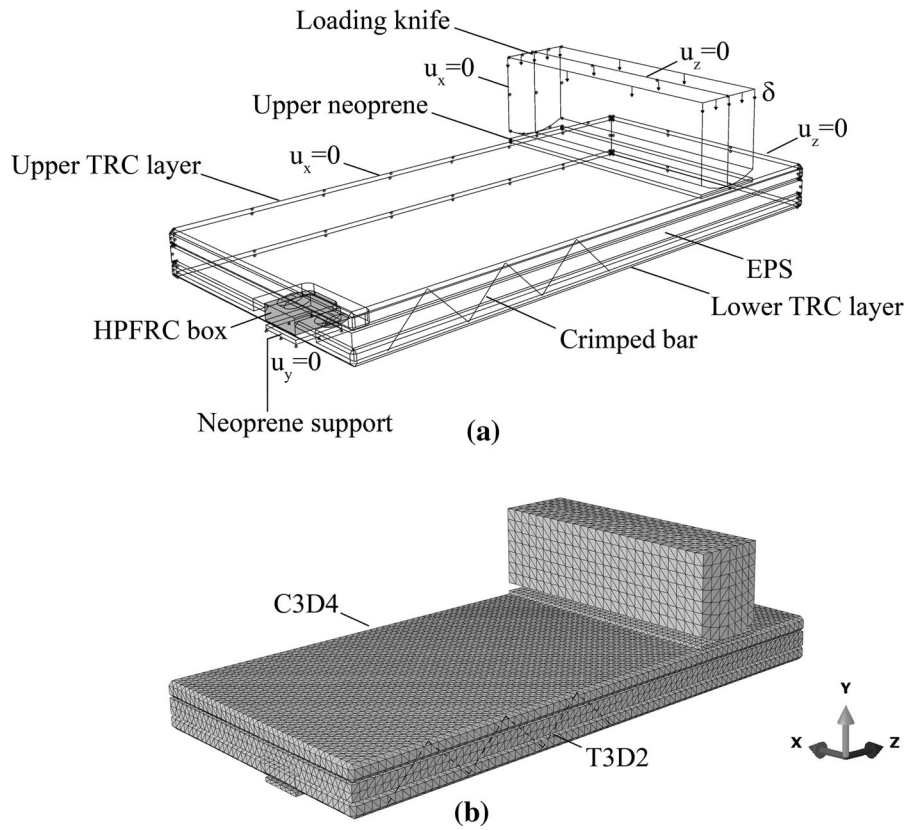

Fig. 9 Model of the panel: geometry with constraints (**a**) and mesh (**b**)—panel V is shown as its geometry is more complex

type of elements, number of elements over the layer thickness and maximum aspect ratio.

4.2 Constitutive laws

In this Section, the constitutive laws adopted for each material are described.

Concerning EPS and TRC, respectively Crushable Foam [28] and Concrete Damage Plasticity [29] models were adopted. These models, in a previous research [22] allowed adequately predicting the behavior of sandwich beams in terms of global response and failure modes after a proper material parameter identification from experimental results. A key point is the modelling of TRC as homogeneous over its thickness, choice that was proved to be reliable and convenient, even if local information were missed.

Elasticity of textile reinforced concrete is defined by means of a Young's modulus of 30 GPa [30] and a Poisson's ratio of 0.2.

As mentioned, the plastic behavior of TRC is implemented using Abaqus Concrete Damage Plasticity model. As no damage curve is introduced, it simply behaves as a plasticity model.

Compressive behavior is assumed elastic-perfectly plastic, with a yield strength equal to the experimental average cubic compressive strength (87.7 MPa).

In tension, a tri-linear stress—strain relationship is introduced (see Fig. 10). This tensile law is obtained starting from the experimental tensile behavior of TRC specimens 400 × 70 × 10 mm^3 tested according to the set-up described in Colombo et al. [31], with repeatability equal to 3. These specimens were cast using the same mortar of the panels and were reinforced with one layer of the same AR-glass fabric. The stress values have been obtained dividing the measured load by the specimen cross-section. Since no direct strain measurement was performed in these tests (only machine cross-head displacement is available), it was not possible to directly compute material strains without including sliding within the clamping devices. For this reason, the actual strains have been computed based on the measurements of the cross-head displacement assuming the same sliding contribution

Table 1 Mesh characteristics

	Nodes	Elements	Elements over the thickness	Max. aspect ratio
V-panel				
Loading knife	1774	8104 (C3D4)	–	2.8
Upper neoprene	885	2450 (C3D4)	1	4.0
Upper TRC layer	6415	19,253 (C3D4)	1	6.1
EPS	20,042	98,352 (C3D4)	6	3.7
Lower TRC layer	6818	20,300 (C3D4)	1	15.5[a]
HPFRC	370	1288 (C3D4)	3	18.9[b]
Neoprene support	98	216 (C3D4)	1	3.0
Crimped bar	103	102 (T3D2)	–	–
Whole model	29,354	150,065	–	–
H-panel				
Loading knife	1823	8201 (C3D4)	–	2.7
Upper neoprene	881	2345 (C3D4)	1	3.0
Upper TRC layer	6745	19,596 (C3D4)	1	7.1
EPS	21,237	104,034 (C3D4)	6	4.1
Lower TRC layer	7152	21,294 (C3D4)	1	15.5[c]
HPFRC	345	1183 (C3D4)	3	11.1[d]
Neoprene support	101	232 (C3D4)	1	3.0
Crimped bar	103	102 (T3D2)	–	–
Whole model	30,949	156,987	–	–

[a]Only the 0.04% of element has a ratio greater than 10.0

[b]Only the 0.70% of element has a ratio greater than 10.0

[c]Only the 0.03% of element has a ratio greater than 10.0

[d]Only the 0.51% of element has a ratio greater than 10.0

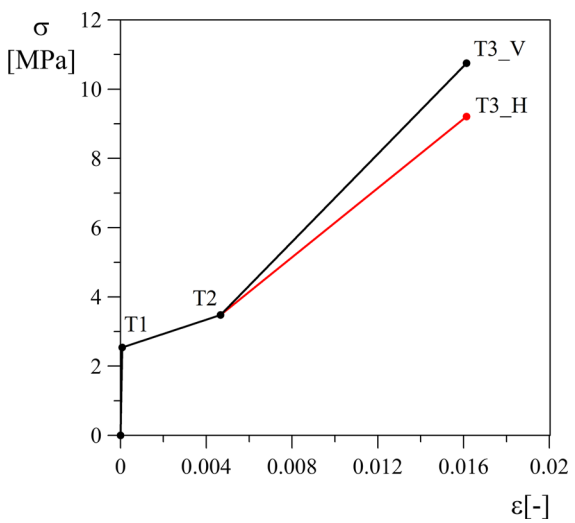

Fig. 10 Tensile constitutive laws adopted for textile reinforced concrete

measured for TRC specimens characterized by the same reinforcement ratio (the procedure is also presented in Colombo et al. [22]).

The following points identify the tensile law: T1, starting of multi-cracking; T2, end of multi-cracking; T3, failure of TRC, due to the brittle failure of the fabric. It is worth noting that, after point T2, only the contributions of fabric and tension stiffening remain active [31].

Point T3 assumes different coordinates for V and H panels, due to the fact that TRC layers are characterized by a different thickness. It is worth remembering that, for TRC specimens, it is possible to define an Efficiency Factor (EF) as the ratio between the specimen peak load and the naked-fabric peak load [31]. For both thicknesses, the failure is governed by the only fabric and, for this reason, if the same EF is considered, the ultimate load and displacement should be equal in the two cases. The difference in thickness

implies a change of the ultimate stress in the constitutive law, but it is supposed not to affect the ultimate elongation because, for such elongation, tension stiffening can be neglected. This consideration leads to a different slope in the third branch.

It is worth to note that a larger thickness may imply a lower EF, which will further reduce the ultimate stress in the constitutive law adopted for H panel. Unfortunately, the lack of a proper experimental investigation on the thickness adopted does not allow providing a reliable prediction of the EF value that, for sake of simplicity, is assumed equal in the two cases.

Concerning expanded polystyrene, the Young's modulus equal to 13.7 MPa and the Poisson's ratio of 0.1 define the elastic behavior. The elastic modulus corresponds to the initial slope of the compressive stress-strain experimental curves [22].

Plasticity is introduced through Crushable Foam model with volumetric hardening. The following parameters have been introduced based on experimental results: yield stress in uniaxial compression ($\sigma_{c0} = 0.19$ MPa), the ratio between the uniaxial and the hydrostatic compressive strength ($k = 1.59$) and the ratio between the hydrostatic tensile and the hydrostatic compressive strength ($k_t = 54.3$) [22]. The hardening law has been introduced based on experimental results in compression. This material model is hardening both in tension and in compression, while EPS is brittle in tension; hence, it was necessary to manually verify that the maximum tensile strength (σ_{t_EPS}) would not be exceeded in the numerical solution in order to exclude a tensile failure of this layer.

Neoprene rubber is supposed to be elastic with a Young's modulus of 0.7 MPa and a Poisson's ratio of 0.49 [32].

Steel constituting the loading knife is considered elastic with a Young's modulus of 210 GPa and a Poisson's ratio of 0.3. The same elastic parameters have been used for the stainless steel constituting the crimped bars (310S); for this material, plasticity is taken into account, introducing a hardening behavior characterized by a yield strength of 205 MPa, an ultimate tensile strength of 515 MPa and an elongation of 40% [33].

4.3 Numerical results

In order to compare the numerical and experimental behavior, the numerical response of vertically cast panel ("V_num") is superimposed on experimental curves in Fig. 4.

As said above, in this figure both V1 and V2 experimental curves were stopped before failure; in any case, it is possible to compare the ultimate load reached by the numerical analysis with the experimental values, which are represented through the horizontal dashed lines.

The model is able to predict the tri-linear panel behavior and the failure load. Comparing experimental and numerical responses, a quite good fitting can be observed, in particular concerning the slope of the second and third branches and the failure load. Concerning the initial branch, the different slope is justified by panel pre-cracking due to previous tests at SLS.

In order to deeply investigate the behavior of the panel, the reaching of relevant points on the material constitutive laws are highlighted in the figure. Points T are those related to the non-linear behavior of TRC in tension (Fig. 10); for these points sub-script "inf" refers to the lower TRC layer, and sub-script "sup" refers to the upper TRC layer. Point E1 indicates the yielding of a compressive strut in the EPS layer [22]. Point S1 indicates the crimped bar yielding.

The investigation allows us to understand that the global tri-linear behavior is governed by the tensile behavior of the lower TRC layer. In fact, the first linear branch ends when the lower TRC layer starts its multi-cracking phase at mid-span (point $T1_{inf}$); the second branch extends up to point $T2_{inf}$, when the multi-cracking of the lower TRC layer ends; finally, the panel collapse is caused by the tensile failure of the lower TRC layer (point $T3_{inf}$). The failure mode obtained in the finite element analysis complies with the failure observed in the experimental tests.

As additional comparison, the numerical results are superimposed to experimental curves in terms of bending moment versus curvature for both H and V panels (see Fig. 5). The higher thickness of TRC layers in H panels leads to a higher first cracking bending moment. The numerical model provides a reliable prediction of the third branch slope, especially in the case of V panels, where a more dense crack pattern is better represented by the smeared hardening uniaxial tensile constitutive law adopted for TRC, that assumes a fixed value of TRC Efficiency Factor and is not able to predict strain localization neither to take into account the energy release at crack formation.

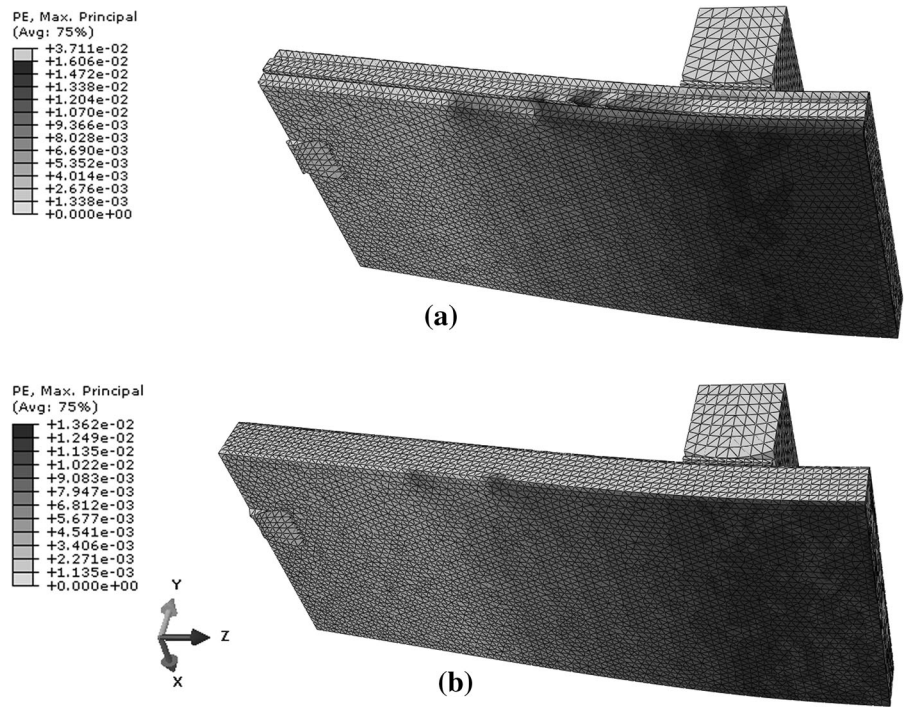

Fig. 11 Plastic strains of panel V (**a**) and panel H (**b**) at failure

The two models provide similar ultimate bending moments because the failure is governed by the TRC rupture, which is driven by the ultimate load of the fabric that is supposed to be the same. In addition, the comparable lever arm and the hardening constitutive law adopted for TRC contribute to obtain small differences in the numerical ultimate bending moment.

The difference between the numerical and experimental ultimate bending moment for H panels can be once again related to the fact that the model is not able to take into account the real crack pattern. FE model considers in both cases a spread plastic strain distribution (Fig. 11) that is more reliable when a more dense crack pattern is available. Moreover, the assumption of the same TRC Efficiency Factor, independently from the thickness, may also lead to an overestimation of the ultimate load of TRC and, therefore, of the ultimate bending moment.

The numerical model well predicts the initial bending stiffness of the un-cracked H panel. Looking at the same Fig. 5, the pre-cracking of V panels can be easily detected by comparing the experimental curves with the un-cracked numerical response. Taking into account the pre-cracking, as lower-bound an additional curve is plotted in the figure ("V_num_r"), representing the numerical response obtained assuming lower TRC as elastic, with a Young's modulus equal to the slope of the final branch of the tensile stress-strain relationship of TRC. It is worth noting that this represents a very rough approximation because this behavior with reduced stiffness is assigned to the entire bottom TRC layer and not only to the cracked region. Moreover, even in the cracked region the initial stiffness is higher with respect to the bared fabric due to tension stiffening exerted by mortar.

In Fig. 11, the plastic strains detected through FE analysis at failure are shown. Looking at the lower TRC layer it is possible to evaluate the extension of the region involved in multi-cracking, finding a good reproduction of experimental tests (see Fig. 8). In addition, especially in sub-figure (a), the compressive strut in expanded polystyrene is recognizable.

5 Conclusions

Bending tests carried out on full-scale sandwich panels made of external textile reinforced concrete layers and inner expanded polystyrene core confirm

the behavior experimented on reduced sandwich samples.

A tri-linear behavior of the panel can be identified, with both the global response and the failure governed by the bottom TRC layer. This evidence also confirms that EPS core is able to transfer shear stresses to the external concrete layers, even if no glue is applied to its external surfaces and the surfaces are characterized by a significant size.

Basing on the sectional responses (bending moment-COD) and on the shear deformations at supports, included in the P-δ_S diagrams, it is possible to state that the casting procedure and the edge detailing do not affect the mechanical behavior of the panel.

The differences registered between V and H panels in terms of ultimate bending moment and crack pattern could be related to the different thickness of the TRC layers, which implies a different energy release at crack formation and, consequently, a different TRC Efficiency Factor.

The numerical model developed in Abaqus and shown in the paper allows a reliable prediction of the global behavior, also in cracked regime, taking into account average values.

This model is able to represent the initial bending stiffness of horizontally cast panels, while an overestimation is registered for vertically cast panels, because these panels were pre-cracked before testing. It is also able to capture the failure modes observed in the experimental tests.

The model provides a reliable prediction of the ultimate bending moment only in the case of V panels. This can be due to the fact that, for V panel, a more realistic Efficiency Factor of TRC has been adopted in the definition of the tensile constitutive law.

In conclusion, the numerical model can be regarded as a valuable tool for the design of this kind of structure.

Acknowledgements The authors would like to thank Gavazzi for the supply of AR glass fabric, Magnetti Bulding for the casting of the panels, Stam for the design of the mould for vertical casting, Halfen for the production of HPFRC boxes and DSC-Erba for the design cooperation. The research was financially supported by the European "EASEE" project, Grant Agreement No. 285540, Thematic Priority: EeB.NMP.2011-3—Energy saving technologies for buildings envelope retrofitting, Starting date of project: 1st of March 2012, Duration: 48 months.

Compliance with ethical standards

Conflict of interest The authors declare that they have no conflict of interest.

References

1. Directive 2010/31/EU of the European Parliament and of the Council of 19 may 2010 on the energy performance of buildings
2. Davies J (2001) Lightweight sandwich construction. Wiley, Hoboken
3. Benayoune A, Samad A, Trikha D, Ali A, Ellinna S (2008) Flexural behaviour of pre-cast concrete sandwich composite panel—Experimental and theoretical investigations. Constr Build Mater 22:580–592
4. Naito C, Hoemann J, Beacraft M, Bewick B (2011) Performance and characterization of shear ties for use in insulated precast concrete sandwich wall panels. J Struct Eng 138:52–61
5. Salmon D, Einea A, Tadros M, Culp T (1997) Full scale testing of precast concrete sandwich panels. ACI Structural Journal 94:354–362
6. Einea A, Salmon DC, Fogarasi GJ, Culp TD, Tadros MK (1991) State-of-the-art of Precast Concrete Sandwich Panels. PCI Journal 36:78–92
7. Hegger J, Horstmann M (2009) Light-weight TRC sandwich building envelopes. Excellence in concrete construction through innovation, pp 187–194
8. Shams A, Horstmann M, Hegger J (2014) Experimental investigations on Textile-Reinforced Concrete (TRC) sandwich sections. Compos Struct 118:643–653
9. Colombo M, di Prisco M, Zecca C (2008) On the coupling of soft materials with thin layers of Glass Fibre Reinforced mortar. In: Proceedings of CCC 2008—challenges for civil construction, Porto, Portugal, on CD
10. Dey V, Zani G, Colombo M, di Prisco M, Mobasher B (2015) Flexural impact response of textile-reinforced aerated concrete sandwich panels. Mater Des 86:187–197
11. di Prisco M, Ferrara L, Lamperti M, Lapolla S, Magri A, Zani G (2012) Sustainable roof elements: a proposal offered by cementitious composites technology. In Fardis MN (ed) Innovative materials and techniques in concrete construction. Springer Netherlands, Dordrecht, pp 167–181
12. di Prisco M, Zani G (2012) Experimental and numerical analysis of advanced cementitious composites for sustainable roof elements. In: Proceedings of the Numerical modeling—Strategies for Sustainable Concrete Structures—Aix-en-Provance, France
13. Ferrara L, Colombo M, di Prisco M, Zecca C (2008) Sandwich panels with glass fiber reinforced surfaces for affordable housing. In: Proceedings of CCC 2008—challenges for civil construction, Porto, Portugal on CD
14. Müller F, Kohlmeyer C, Schnell J (2012) Load-bearing behaviour of sandwich strips with XPS-core and reinforced HPC-facings. In: Ultra-high performance concrete and nanotechnology in construction, proceedings of hipermat 2012—3rd international symposium on UHPC and

nanotechnology for high performance construction materials. Kassel University Press, Kassel, pp 781–788
15. Vervloet J, Van Itterbeeck P, Verbruggen S, El Kadi M, De Munck M, Wastiels J, Tysmans T (2019) Experimental investigation of the buckling behaviour of Textile Reinforced Cement sandwich panels with varying face thickness using Digital Image Correlation. Constr Build Mater 194:24–31
16. Williams Portal N, Flansbjer M, Zandi K, Wlasak L, Malaga K (2017) Bending behaviour of novel Textile Reinforced Concrete-foamed concrete (TRC-FC) sandwich elements. Compos Struct 177:104–118
17. Colombo IG, Colombo M, di Prisco M, Salvalai G, Sesana MM (2018) TRC sandwich panel for energy retrofitting exposed to environmental loading, ACI SP-326, pp 76.1–76.10
18. Colombo IG (2015) Multilayer precast façade panel: structural optimization for energy retrofitting. PhD thesis. PhD in Structural, Seismic and Geotechnical Engineering, Politecnico di Milano (Department of Civil and Environmental Engineering)
19. Colombo IG, Colombo M, di Prisco M (2015) Tensile behavior of textile reinforced concrete subjected to freezing-thawing cycles in un-cracked and cracked regimes. Cem Concr Res 73:169–183. https://doi.org/10.1016/j.cemconres.2015.03.001
20. Colombo IG, Colombo M, di Prisco M (2015) Bending behaviour of Textile Reinforced Concrete sandwich beams. Constr Build Mater 95:675–685
21. Colombo IG, Colombo M, di Prisco M (2015) TRC precast façade sandwich panel for energy retrofitting of existing buildings. ACI SP-305, pp 30.1–30.10
22. Colombo IG, Colombo M, di Prisco M, Pouyaei F (2018) Analytical and numerical prediction of the bending behaviour of textile reinforced concrete sandwich beams. Journal of Building Engineering 17:183–195. https://doi.org/10.1016/j.jobe.2018.02.012
23. Colombo IG, Colombo M, di Prisco M (2016) TRC multilayer precast façade panel: structural behavior in freezing-thawing condition. In: Proceedings of the II international conference on concrete sustainability ICCS16, Madrid, June 13th–15th, 2016
24. EN 196-1. 2005. Methods of testing cement—part 1: determination of strength
25. Colombo IG, Colombo M, Magri A, Zani G, di Prisco M (2011) Textile reinforced mortar at high temperatures. In: Proceedings of "Protect 2011—performance, protection and strengthening of structures under extreme loading, Lugano, August 30th–September 1st, 2011
26. UNI EN 13163 (2009) Thermal insulation products for buildings—factory made products of expanded polystyrene (EPS)—specification
27. Hegger J, Will N, Curbach M, Jesse F (2004) Tragverhalten von textilbewehrtem Beton. Beton- und Stahlbetonbau 99:452–455
28. Deshpande VS, Flek N (2000) Isotropic Constitutive Model for Metallic Foams. J Mech Phys Solids 48:1253–1276
29. Lee J, Fenves G (1998) Plastic-Damage Model for Cyclic Loading of Concrete Structures. Journal of Engineering Mechanics 124(8):892–900
30. Brameshuber W, Brockmann T, Curbach M, Meyer C, Vilkner G, Mobasher B et al (2006) Textile reinforced concrete—state-of-the-art. In Brameshuber W (ed) Report of RILEM Technical Committee 201-TRC. RILEM Publications
31. Colombo IG, Magri A, Zani G, Colombo M, di Prisco M (2013) Textile Reinforced Concrete: experimental investigation on design parameters. Mater Struct 46(11):1933–1951
32. Materials Data Book (2003) Cambridge University Engineering Department
33. ASTM International A473—17a: Standard specification for stainless steel forgings